# Equivalent Diagonal Strut Method for Masonry Walls in Pinned Connection and Multi-Bay Steel Frames

**Sayed Mohamad Motovali Emami[1], Majid Mohammadi[2*], and Paulo B. Lourenço[3]**

1. Ph.D. Candidate, International Institute of Earthquake Engineering and Seismology (IIEES), Tehran, Iran
2. Associate Professor, Structural Engineering Research Center, International Institute of Earthquake Engineering and Seismology, Tehran, Iran,
* Corresponding Author; email: m.mohammadigh@iiees.ac.ir
3. Professor, ISISE, University of Minho, Department of Civil Engineering, Portugal

**Received:** 09/07/2017
**Accepted:** 21/08/2017

## ABSTRACT

*Equivalent compression strut is one of the most prevalent approaches recommended in seismic codes to simulate infill panels in the frames. The mechanical parameters of infilled frames, such as strength and stiffness, are controlled by material properties, thickness and width of equivalent strut. The strut width depends on the contact length between the infill and the frame. Previous studies have shown that the connection rigidity of the surrounding frame affects the contact length and consequently the response of infilled frame. Parametric finite element analyses have been carried out to investigate the influence of frame connection rigidity on the behavior of infill walls using ABAQUS environment. The finite element models were verified based on the results of experimental data. It is shown that the stiffness and strength of infill panel in pinned connection steel frame are 0.9 and 0.8 times of those in rigid connection frame, respectively. The results of parametric finite element analyses were validated using equivalent strut method. Moreover, it is shown that the equivalent diagonal struts in multi-bay frame have the same properties of strut in one-bay frames for both rigid and pinned connections ones.*

**Keywords:**
Infill wall; Pinned connection frame; Equivalent strut model; Multi-bay infilled frame; ABAQUS; FEM

## 1. Introduction

Masonry-infill panels can be found as interior and exterior walls in framed structures. Since they are normally considered as architectural elements, their presence is often ignored by structural engineers. It has been found experimentally that the stiffness and strength of an infilled frame cannot be obtained by the addition of the stiffness and strength of the frame and the wall. Both the stiffness and strength of the assemblage are affected by the interaction between the frame and the wall.

Ignoring the effect of the infill in stiffening and strengthening the surrounding frame is not always a conservative approach, since the stiffer the building, usually, the higher seismic loads it attracts. Therefore, several models have been proposed to consider the effects of infill panels on structures in previous researches. One of these models is the equivalent diagonal strut model that was firstly pro-posed by Polykov [1] and Holmes [2]. In this model, the infill panel is replaced by an equivalent diagonal strut that

is acting in compression to resist the lateral loading. Several studies such as Staf-ford-Smith and Carter [3], and Mainstone [4] have been carried out to modify equivalent strut method. This model is also recommended by seismic guidelines such as FEMA356 [5] and ASCE41-06 [6] to model the infills. In most cases, the equivalent strut model replacing in frame can estimate the stiffness and strength of infilled frames, acceptably. From other point of view, these models were obtained based on experiments and analyses on which the surrounding frames have rigid connections, while there are a lot of frames with pinned connections filled by masonry walls. A number of studies have been focused on the infilled steel frames which had not rigid connections of beam to column. Dawe and Seah [7] found out that the infill in a pinned connection frame has less stiffness and strength as well as lower ductility, compared with one in a rigid connection frame. Flanagan and Bennet [8] performed a series of experiments on steel frames with structural clay tile infills. The steel beams connected to column by double clip angles. The results show that the stiffness and strength of the specimens were about half of the values calculated by Mainstone [4] formula. Motovali Emami and Mohammadi [9] have experimentally shown that the stiffness and strength of infilled frame with pinned connection are lower than those of infilled rigid frames. Since the be-havior of infilled frame are controlled by the response of both infill wall and surrounding frame, the reduction in stiffness and strength may be attributed to lower rigidity of frame or decrease in contact length between infill and frame while lateral loading or both of them. Therefore, using the equivalent strut method to determine the behavior of infilled frames with pinned connections is doubtful.

In addition, various studies have been intended to clarify the effect of number of bays on the behavior infilled frame. Murthy and Hendry [10] found that the stiffness of infilled frame increase non-linearly by increasing the bays number of infilled frame. Mosalam et al. [11] tested five re-duced-scaled masonry infilled single and two-bay steel frames. They observed that the maximum strength and stiffness of double-bay specimen were 2 and 1.7 times of those of single-bay infilled frame. In 2002, a study by Al-Chaar et al. [12] on half-scaled multi-bay infilled RC frames sub-jected to in-plane loading demonstrated that the maximum strength of infilled frame have not linear relation with the number of bays. It can also be inferred that the behavior of multi-bay infill speci-men have strongly depended on the method of application of lateral loading to the infilled frame. Motovali Emami [13] experimentally informed that the strength of two-bay masonry infilled steel frame was 1.9 times of strength of single-bay specimen; however, stiffness increase by 2 to 1.5 times depends on the connection types of surrounding frame.

This study intends to clarify the effect of frame connection rigidity and number of bays on the lat-eral response on infill wall. For this purpose extensive numerical finite element masonry infilled frames were analyzed by pushover method using ABAQUS [14] finite element program. These models included single and multi-bay infilled steel frames with rigid and pinned connections. The finite element infilled frame was verified by experimental results of similar infilled frame specimen performed by Motovali Emami and Mohammadi [15]. Afterward, the results obtained from numerical investigation were applied to control the efficiency of the equivalent diagonal strut methodology.

## 2. Theoretical Background for Modeling

To obtain the behavior of infilled frame models, nonlinear static analysis was conducted using commercial software ABAQUS/Explicit [14]. Energy balance check and mass scaling were applied to ensure quasi static behavior while using dynamic explicit analysis. In the following, the material for modelling masonry and interface mortar will be explained.

### *2.1. Constitutive Models*

#### 2.1.1. Concrete Damage Plasticity

To simulate the nonlinear response of the masonry units, the CDP (concrete damage plasticity) model available in ABAQUS was used. CDP model has been developed to predict the behavior of concrete and other quasi-brittle materials such as rock and mortar under cyclic loading. Cracks in tension or crushing in compression are the main failure modes of this model. The model is based on primary models proposed by Lubliner et al. [16] and Lee and Fenves

[17]. The tension and com-pression damage from micro to macro cracking can be tracked separately in this model. CDP model assumes that the uniaxial compressive and tensile response of concrete is characterized by damaged plasticity as shown in Figure (1).

### 2.1.2. Cohesive Surface-Base Element

Generally, cohesive interactions are a function of displacement separation between the edges of po-tential cracks. The concept of cohesive zone was employed by Dugdale [18] for the first time. Needleman [19] recognized that cohesive elements are partially useful when interface strength are relatively weak compared to the adjoining materials. Composite part is an example for modeling with the adhesive bonded interfaces. Adhesive bonded interface is appropriate to model the separation between two initially bonded surfaces. The mech-anical constitutive behavior of cohesive elements can be defined in three methods: (1) uniaxial stress-based, (2) continuum-based and (3) traction-separation constitutive model. Where two bodies are connected by a third part material like glue, the continuum-based modeling is appropriate for the adhesive. In this case, glue should be considered with a finite thickness. The mechanical properties of adhesive material were employed directly in the model from the experimental results [13]. The cohesive elements can be applied in situations where cracks are expected to propagate. In this model, cracks are restricted to develop along the layers at the head and bed joints. Prior to damage, the cohesive behavior follows a linear traction-separation law and progressive degradation of the bond stiffness leads to the bond failure. Once a damage initiation in the interface element is met, damage will take place based on the user defined damage factor. A typical traction-separation response is presented in Figure (2a). In the elastic part, the traction stress vector consists of normal, $t_n$ and two shear traction components $t_s$; $t_t$. These components represent mode I, II and III of fracture modes shown in Figure (2b). Besides, in this model $\delta_n^0, \delta_s^0$ and $\delta_t^0$ represent the corresponding initial separation caused by pure normal, in plane and out-of-plane shear stresses, respectively. The second part of traction-separation response shows the damage propagation of bond that can be determined in different ways in ABAQUS [14]. The maximum nominal stress (MAXS) for damage propagation was selected here. The damage ini-tiates when

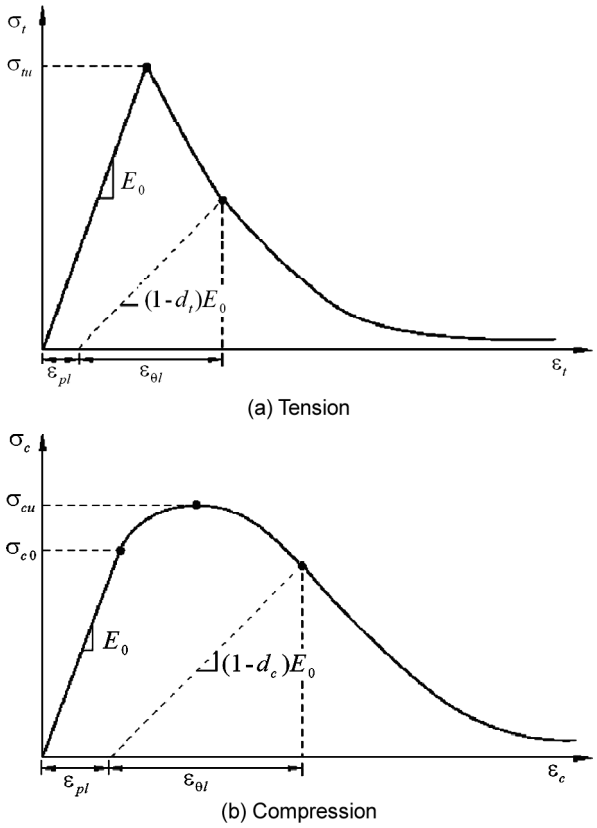


**Figure 1.** Response of CDP model to uniaxial loading [14].

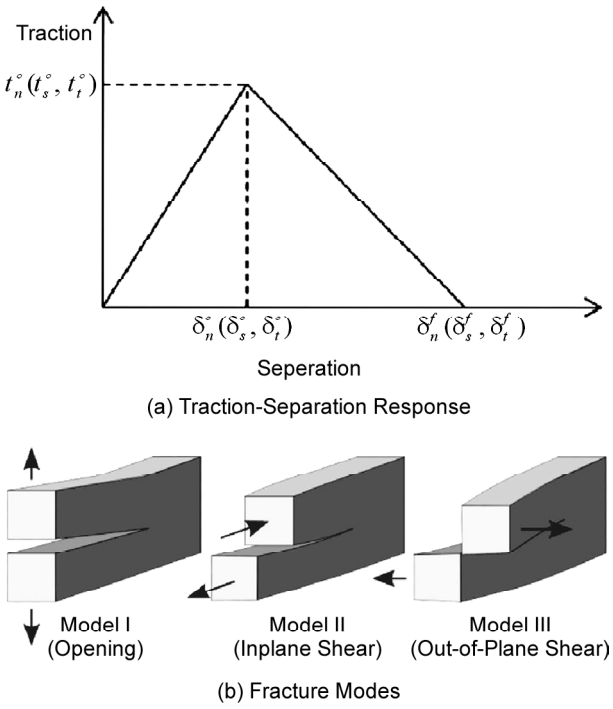


**Figure 2.** Typical traction-separation behavior and fracture modes [20].

the maximum nominal stress ratio reaches a value of one. Damage evolution in this model describes the degradation of the cohesive stiffness. For this purpose, the maximum separation at the end of graph can be specified. Post damage-initiation separation was used to consider the damage evolution in the present study (i.e. $\delta_n^f$, $\delta_s^f$ and $\delta_t^f$). In this study, the above-mentioned values were calculated using data of masonry prism testing as well as try and error to achieve the best result.

Cohesive elements are used to bond two bodies and they degrade after applying load due to the tensile or shear deformation. Subsequently, the two bonded component come into a contact after debonding. Therefore, Coulomb frictional contact behavior is also defined in the current model. Coulomb friction describes the interaction of contacting surfaces and the model characterizes the frictional behavior using a coefficient of friction, μ. It is important to avoid components penetration after forming the contact, especially for the normal behavior of contacts. This allows the as-semblages to take apart in presence of the critical force. For the presented study, general contact (hard contact) was used to avoid penetration of bricks and infill to frame together, available in ABAQUS. The coefficient of friction can be defined based upon slip-rate data. In this study, contact-pressure dependent behavior was used based on the results from the shear test assemblages. The tangential motion is zero until the surface traction reaches a critical shear stress value which is dependent upon the normal contact pressure, according to Equation (1):

$$\tau_c = \mu p \quad (1)$$

where μ is the coefficient of friction and $p$ is contact pressure between the two surfaces. This equation introduces the limiting frictional shear stress for the contacting surfaces. The contacting surfaces do not slip until the shear stress across their interface reaches the limiting frictional shear stress, as depicted in Figure (3).

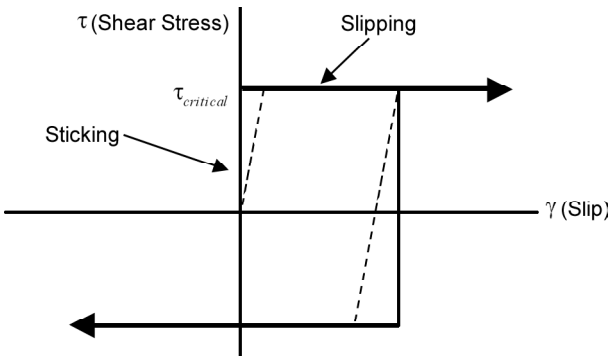


**Figure 3.** Frictional behavior [14].

## 3. Numerical Verification

### *3.1. Experimental Model*

The capability of the finite element model as interface element has been validated with the experi-mental data of masonry infilled steel frame test by Motovali Emami and Mohammadi [15]. The half-scaled specimen M-RC that was a moment-resisting steel frame with brick masonry infill panel was modeled in ABAQUS. The schematic view of the M-RC specimen is illustrated in Figure (4). The beams and column sections of specimen were IPBL120 and IPBL180, respectively. The masonry wall with 95 mm thickness filled the steel frame. The average mechanical properties of surrounding frame steel as well as masonry prism are available in Tables (1) and (2). The specimen was tested under cyclic reversal lateral loading and the result of pushover analysis of finite element model is compared with backbone of experimental result.

### *3.2. FE Model*

#### 3.2.1. Concrete Damage Plasticity Parameters

Table (3) shows the material properties which were used for modeling the masonry infill wall.

**Table 1.** Mechanical properties of steel.

| Module of Elasticity (MPa) | Yield Stress ($\sigma_y$) (MPa) | Ultimate Stress ($\sigma_u$) (MPa) | $\varepsilon_h$ | $\varepsilon_u$ |
|---|---|---|---|---|
| 171000 | 313.8 | 484.4 | 0.017 | 0.141 |

**Table 2.** Mechanical properties of masonry prism.

| Module of Rapture (MPa) | Poisson's Ratio | Compressive Strength (MPa) | Tensile Strength (MPa) | Shear Strength (MPa) | Coefficient of Friction |
|---|---|---|---|---|---|
| 1892.2 | 0.15 | 9.9 | 0.69 | 0.3 | 0.75 |

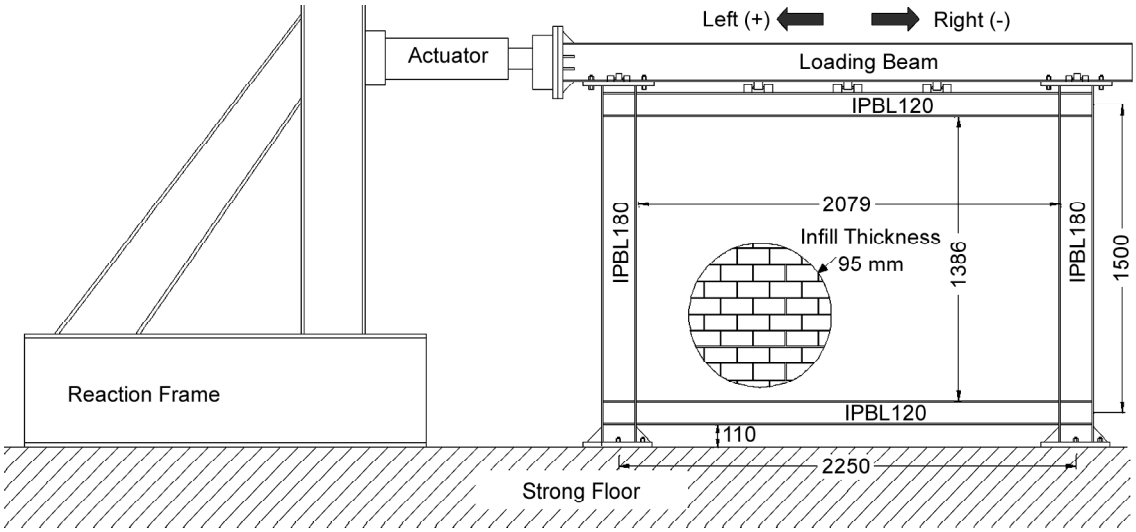


**Figure 4.** Schematic view of test setup, dimension in mm [15].

**Table 3.** Material properties of masonry for CDP model.

| Mass Density (kg/m$^3$) | Elasticity | | Plasticity | | | | |
|---|---|---|---|---|---|---|---|
| | Young's Modules (MPa) | Poisson's Ratio υ | Dilation Angle ψ | Eccentricity | $f_{b0}/f_{c0}$ | $K$ | Viscosity Parameter |
| 1812 | 1892 | 0.15 | 20 | 0.1 | 1.16 | 0.66 | 0 |

The plasticity characteristics of material need different types of experimental tests that are beyond the scope of this research. In the absence of such data, the plasticity parameters were determined indirectly by trial and error in the calibration process, and by use of common values recommended in the literature. Modulus of elasticity and the compressive behavior of CDP model were extracted from result of masonry prism test [13]. Table (4) shows the yield stress versus the inelastic strain and cracking strain calculated from the prism test.

**Table 4.** Compressive and tensile behavior of the masonry for CDP model.

| Concrete Damage Plasticity | | | |
|---|---|---|---|
| Compressive Behavior | | Tensile Behavior | |
| Yield Stress (MPa) | Inelastic Strain | Yield Stress (MPa) | Cracking Strain |
| 6.92 | 0 | 0.69 | 0 |
| 8.0 | 0.00033 | 0.54 | 0.00011 |
| 9.68 | 0.00177 | 0.36 | 0.00029 |
| 9.90 | 0.00287 | 0.25 | 0.00042 |
| 9.68 | 0.00418 | 0.17 | 0.00055 |
| 8.63 | 0.00644 | 0.12 | 0.00067 |
| 7.28 | 0.00842 | 0.09 | 0.00078 |
| 4.28 | 0.01193 | 0.07 | 0.00088 |

### 3.2.2. Joints Cohesive Behavior Parameters

Cohesive behavior of mortar was defined based on information presented in Table (5). Mortar is the only source of bond resistance against shear forces along the bed joints of bricks as well as infill and frame. Average shear strength of prism specimens reported in [13] were also used for mode II that is called shear I in Table (5). Since there is no out-of-plane shear in force applied to the tested specimen, to simulate the mode III (shear II), shear value of masonry was taken equal to zero in this mode. Plastic displacement and Exponential parameter values, which employed in the strength degradation of mortars, were calculated based on trial and error to obtain reasonable result. ABAQUS use Equation (2) to calculate cohesive degradation:

$$D = 1 - \left\{ \frac{\delta_m^0}{\delta_m^{\max}} \right\} \left\{ 1 - \frac{1 - \exp(-\alpha(\frac{\delta_m^{\max} - \delta_m^0}{\delta_m^f - \delta_m^0}))}{1 - \exp(-\alpha)} \right\} \quad (2)$$

where $\delta_m^0, \delta_m^{\max}$ and $\delta_m^f$ are displacement imposed to the mortar at beginning of the test, during the test and while the mortar fully degraded, respectively.

**Table 5.** Cohesive behavior of brick to brick and infill to frame joints.

| Surface | Contact | | | | | | | | | |
|---|---|---|---|---|---|---|---|---|---|---|
| | Tangential Behavior | Normal Behavior | Cohesive Behavior | | | | | | | |
| | | | Traction-Separation Behavior | | | Damage | | | | |
| | | | Stiffness Coefficients (MN/m) | | | Initiation (MPa) | | | Evolution | |
| | | | $K_{nn}$ | $K_{ss}$ | $K_{tt}$ | Normal | Shear I | Shear II | Plastic Displacement (mm) | Exponential Parameter |
| Brick-Brick | 0.75 | Hard Contact | 11 | 11 | 11 | 0.15 | 0.2 | 0.2 | 1.5 | 2 |
| Infill-frame | 0.57 | Hard Contact | 11 | 11 | 11 | 0.1 | 0.15 | 0.15 | 1 | 10 |

Moreover, α is exponential parameter of degradation function. Figure (5) shows the schematic traction-separation behavior of mortar in the model.

Since the traction-separation graph is linear, the slope of each line called stiffness coefficient is assumed to be 10 MN/m. Theatrically, this stiffness in normal direction is module of elasticity of mortar divided by thickness of mortar, which can be calculated based on Equation (3) (for more information one can refer to [13]):

$$\Rightarrow K_{nn} = \frac{E_j}{t} = \frac{2E_u E_m}{3h(2E_u - E_m) + 4tE_u} \quad (3)$$

where $E_m$ and $E_u$ are modules of elasticity of masonry prism and brick, respectively. Moreover, $h$ and $t$ are thickness of brick unit and mortar joint, respectively. For simplicity, in the traction-separation model the same stiffness in the normal and shear directions were assumed.

Contact assumed to be zero thickness and therefore hard contact was assigned for normal behavior of contact. It is supposed that "Hard" contact refers to an interaction without any softening, in other words, no penetration of the surfaces can occur in the model. Moreover, the friction coefficient of brick masonry and brick to steel is chosen 0.75 and 0.57, respectively, in which the best fit was captured in this study.

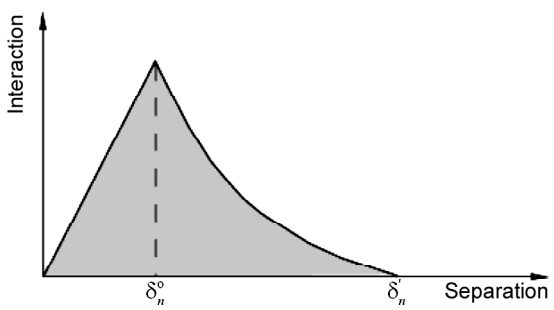


**Figure 5.** Schematic view of mortar degradation function [14].

### *3.3. Model Outputs*

The result of finite element infilled frame model was accepted based on two assumptions. (1) Acquire the best fit of experimental pushover; (2) Capture the same failure modes of experimental and numerical model. Figure (6) shows the load-displacement relationship of the infilled frame from the numerical analysis and experimental test. One can conclude that the FEM model was able to predict the stiffness and strength of masonry infilled steel frame with good agreement.

The crack patterns of infill panels in the experimental and FEM models are depicted in Figure (7). As can be seen, the infill failure modes of both models are inclined cracking in a way that two com-pression strut are formed in the infill. On the other hand, the same failure mode is occurred in the experimental and numerical infilled frame. As a result, one can confirm that, the finite element numerical model in this study can capture the nonlinear behavior of masonry infilled steel frame in reliable range.

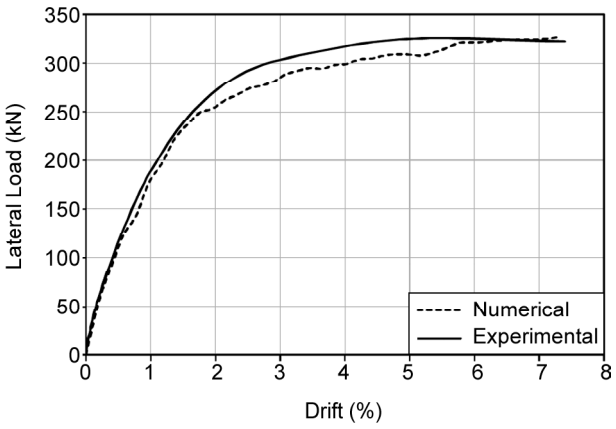


**Figure 6.** Comparison between experimental and numerical capacity curves.

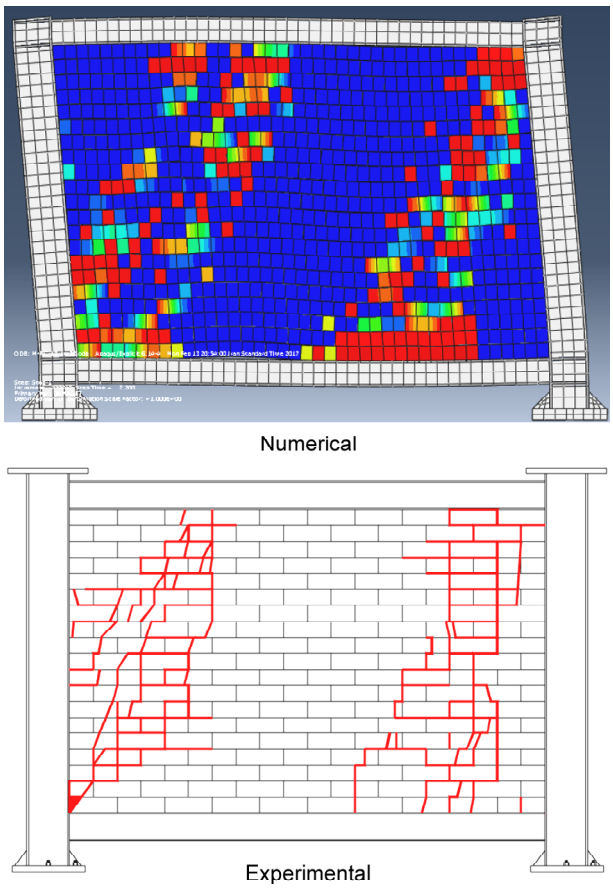


**Figure 7.** Infill failure modes of experimental and numerical models.

**Table 6.** Infilled frames models and their parameters.

| ID | Beam | Column | Connection Type | Aspect Ratio ($L/H$) | $\lambda L$ | Bay No. |
|---|---|---|---|---|---|---|
| 1 | IPBL 120 | IPBL180 | Rigid | 0.5 | 2.4 | 1 |
| 2 | IPBL 120 | IPBL180 | Pinned | 0.5 | 2.4 | 1 |
| 3 | IPBL 120 | IPBL180 | Rigid | 1 | 2.4 | 1 |
| 4 | IPBL 120 | IPBL180 | Pinned | 1 | 2.4 | 1 |
| 5 | IPBL 120 | IPBL180 | Rigid | 1.5 | 2.4 | 1 |
| 6 | IPBL 120 | IPBL180 | Pinned | 1.5 | 2.4 | 1 |
| 7 | IPBL 120 | IPBL180 | Rigid | 2 | 2.4 | 1 |
| 8 | IPBL 120 | IPBL180 | Pinned | 2 | 2.4 | 1 |
| 9 | IPBL 100 | IPBL 120 | Rigid | 0.5 | 3.4 | 1 |
| 10 | IPBL 100 | IPBL 120 | Pinned | 0.5 | 3.4 | 1 |
| 11 | IPBL 100 | IPBL 120 | Rigid | 1 | 3.4 | 1 |
| 12 | IPBL 100 | IPBL 120 | Pinned | 1 | 3.4 | 1 |
| 13 | IPBL 100 | IPBL 120 | Rigid | 1.5 | 3.4 | 1 |
| 14 | IPBL 100 | IPBL 120 | Pinned | 1.5 | 3.4 | 1 |
| 15 | IPBL 100 | IPBL 120 | Rigid | 2 | 3.4 | 1 |
| 16 | IPBL 100 | IPBL 120 | Pinned | 2 | 3.4 | 1 |
| 17 | IPBL 120 | IPBL180 | Rigid | 1.5 | 2.4 | 2 |
| 18 | IPBL 120 | IPBL180 | Pinned | 1.5 | 2.4 | 2 |
| 19 | IPBL 120 | IPBL180 | Rigid | 1.5 | 2.4 | 3 |
| 20 | IPBL 120 | IPBL180 | Pinned | 1.5 | 2.4 | 3 |

## 4. Parametric analysis

To investigate the effects of connection rigidity and number of bays on the behavior of masonry infilled frames, sensitivity analysis was carried out based on the above-mentioned infilled frame modeling. For this purpose, 40 models included 20 masonry-infilled steel frames as well as their corresponding 20 surrounding frames was modeled, which only the infilled frames are listed in Table (6). As it can be seen, the variable parameters of the models are frame connection type (rigid and pinned), infill aspect ratios ($L/H$), relative rigidity of infill to frame ($\lambda L$) and number of bays. It should be noted that the thickness of all infill is 9.5 cm. The relative stiffness of infill to frame is a non-dimensional parameter, which can be calculated based on the formula proposed by Mainstone [4]:

$$\lambda h = h_{col}\left[\frac{E_{me}t_{\inf}\sin 2\theta}{4E_{fe}I_{col}h_{\inf}}\right]^{\frac{1}{4}} \quad (4)$$

where $h_{col}$ is the height of the column, $E_{me}$ is the modulus of elasticity of the infill panel, $t_{inf}$ is the thickness of the infill, $\lambda$ is the angle of the infill diagonal with respect to the horizontal, $E_{fe}$ and $I_{col}$ are the modulus of elasticity and flexural rigidity of the columns, respectively and $h_{inf}$ is the height of the infill panel.

Nonlinear static pushover analysis was performed on all models up to the drift of 4% using ABAQUS software. To study the effect of connection rigidity and number of bays, initial stiffness and strength of infilled frame and their corresponding bare frame were calculated. In addition, the behavior of infill panels was determined by subtracting the pushover curve of infilled frame from its bare frame.

### *4.1. Effect of Connection Rigidity*

Table (7) shows the ratio of Pinned Connection (PC) to Rigid Connection (RC) initial stiffness for infilled frames, bare frames and infill contributions with respect to their aspect ratios and $\lambda L$. The mean value of PC-to-RC stiffness for infilled frame is 0.86 with a COV of 6.06%. As it can be seen, the reduction in the initial stiffness of infilled frames as a result of frame connection type is attribut-ed to

both reductions in frame rigidity and infill-frame interaction. On the other hand, the mean PC-to-RC stiffness ratio of the frame is 0.81 with COV of 8.16% while for the infill contribution is 0.91 with COV of 5.61%. One can conclude that the change in the frame connection from rigid to pinned will result in a reduction around 10% in the stiffness of infill panel that is imparted to infilled frame.

**Table 7.** Effect of frame connection types on initial stiffness.

| $\lambda L$ | Aspect Ratio (L/H) | PC-to-RC Stiffness Ratio | | |
|---|---|---|---|---|
| | | Infilled Frame | Bare Frame | Infill Contribution |
| 2.4 | 0.5 | 0.80 | 0.80 | 0.83 |
| | 1 | 0.94 | 0.90 | 0.94 |
| | 1.5 | 0.86 | 0.85 | 0.87 |
| | 2 | 0.93 | 0.90 | 0.97 |
| 3.4 | 0.5 | 0.85 | 0.78 | 0.96 |
| | 1 | 0.83 | 0.73 | 0.92 |
| | 1.5 | 0.80 | 0.76 | 0.85 |
| | 2 | 0.85 | 0.74 | 0.91 |
| Avg. | | 0.86 | 0.81 | 0.91 |
| Std. | | 0.05 | 0.07 | 0.05 |
| COV (%) | | 6.06 | 8.16 | 5.61 |

The strength ratio of pinned connection to rigid connection models for infilled frames, bare frames and infill contributions are listed in Tables (8) to (10), respectively. The strength values are extracted from pushover curves for the drifts of 1.35%, 1.67%, 2% and 2.5% to cover the immediate occupancy to life safety performance levels. According to Iranian seismic code [21], 2% and 2.5% of inter-story drifts correspond to life safety limit state, and 0.67 times of the deformation limit in Life Safety (LS) is attributed to immediate occupancy (IO) limit state [22]. Table (8) shows that the strength of pinned

**Table 8.** Effect of frame connection types on the strength of infilled frame.

| Infilled Frame | | | | | | | | |
|---|---|---|---|---|---|---|---|---|
| $\lambda L$ | Aspect Ratio (L/H) | PC-to-RC Strength Ratio | | | | Avg. | Std. | COV (%) |
| | | Drift (%) | | | | | | |
| | | 1.35 | 1.67 | 2 | 2.5 | | | |
| 2.4 | 0.5 | 0.88 | 0.90 | 0.91 | 0.91 | 0.90 | 0.02 | 1.78 |
| | 1 | 0.85 | 0.86 | 0.85 | 0.89 | 0.86 | 0.02 | 2.39 |
| | 1.5 | 0.86 | 0.86 | 0.86 | 0.85 | 0.86 | 0.00 | 0.34 |
| | 2 | 0.90 | 0.88 | 0.84 | 0.85 | 0.87 | 0.03 | 2.98 |
| 3.4 | 0.5 | 0.86 | 0.88 | 0.91 | 0.91 | 0.89 | 0.03 | 2.93 |
| | 1 | 0.80 | 0.81 | 0.83 | 0.84 | 0.82 | 0.02 | 2.48 |
| | 1.5 | 0.84 | 0.84 | 0.86 | 0.85 | 0.85 | 0.01 | 1.28 |
| | 2 | 0.88 | 0.89 | 0.90 | 0.85 | 0.88 | 0.02 | 2.46 |
| | Avg. | 0.86 | 0.86 | 0.87 | 0.87 | **0.87** | | |
| | Std. | 0.03 | 0.03 | 0.03 | 0.03 | | **0.03** | |
| | COV (%) | 3.36 | 3.44 | 3.57 | 3.46 | | | **3.35** |

**Table 9.** Effect of frame connection rigidity on the strength of bare frame.

| Bare Frame | | | | | | | | |
|---|---|---|---|---|---|---|---|---|
| $\lambda L$ | Aspect Ratio (L/H) | PC-to-RC Strength Ratio | | | | Avg. | Std. | COV (%) |
| | | Drift (%) | | | | | | |
| | | 1.35 | 1.67 | 2 | 2.5 | | | |
| 2.4 | 0.5 | 0.86 | 0.88 | 0.89 | 0.91 | 0.89 | 0.02 | 2.41 |
| | 1 | 0.86 | 0.87 | 0.86 | 0.88 | 0.87 | 0.01 | 0.73 |
| | 1.5 | 0.83 | 0.86 | 0.86 | 0.86 | 0.85 | 0.02 | 1.77 |
| | 2 | 0.90 | 0.89 | 0.88 | 0.89 | 0.89 | 0.00 | 0.51 |
| 3.4 | 0.5 | 0.87 | 0.87 | 0.87 | 0.91 | 0.88 | 0.02 | 2.28 |
| | 1 | 0.82 | 0.86 | 0.86 | 0.87 | 0.85 | 0.02 | 2.33 |
| | 1.5 | 0.88 | 0.85 | 0.89 | 0.91 | 0.88 | 0.02 | 2.74 |
| | 2 | 0.89 | 0.88 | 0.89 | 0.89 | 0.89 | 0.00 | 0.49 |
| | Avg. | 0.86 | 0.87 | 0.88 | 0.89 | **0.87** | | |
| | Std. | 0.03 | 0.01 | 0.02 | 0.02 | | **0.02** | |
| | COV (%) | 2.97 | 1.61 | 1.74 | 2.15 | | | **2.32** |

**Table 10.** Effect of frame connection types on the strength of infill contribution.

| Infilled Contribution | | | | | | | | |
|---|---|---|---|---|---|---|---|---|
| | | PC-to-RC Strength Ratio | | | | | | |
| $\lambda L$ | Aspect Ratio (L/H) | Drift (%) | | | | Avg. | Std. | COV (%) |
| | | 1.35 | 1.67 | 2 | 2.5 | | | |
| 2.4 | 0.5 | 0.99 | 1.0 | 1.0 | 0.95 | 0.99 | 0.03 | 3.41 |
| | 1 | 0.81 | 0.84 | 0.84 | 0.96 | 0.86 | 0.07 | 7.63 |
| | 1.5 | 0.94 | 0.86 | 0.86 | 0.83 | 0.87 | 0.05 | 5.37 |
| | 2 | 0.91 | 0.81 | 0.66 | 0.73 | 0.78 | 0.11 | 13.82 |
| 3.4 | 0.5 | 0.83 | 0.91 | 1.0 | 0.92 | 0.93 | 0.09 | 9.41 |
| | 1 | 0.78 | 0.74 | 0.79 | 0.82 | 0.78 | 0.03 | 4.14 |
| | 1.5 | 0.79 | 0.82 | 0.81 | 0.74 | 0.79 | 0.03 | 4.27 |
| | 2 | 0.85 | 0.89 | 0.90 | 0.75 | 0.85 | 0.07 | 8.17 |
| | Avg. | 0.84 | 0.83 | 0.81 | 0.80 | **0.82** | | |
| | Std. | 0.08 | 0.08 | 0.12 | 0.10 | | **0.09** | |
| | COV (%) | 9.0 | 10.11 | 15.38 | 11.82 | | | **11.26** |

connection infilled frames is lower than those of rigid connection infilled frame with an overall mean PC-to-RC ratio of 0.87 with a COV of 3.35%. According to Table (9), as one expected, the strength of rigid frame to the pinned frame is declined by 13% and the mean PC-to-RC ratio is 0.87 with a COV of 2.32%. As it is mentioned before, to investigate the effect of connection rigidity of surrounding frame on the behavior of infill wall, the strength of infill is calculated by subtracting the response of infilled frame from bare frame. Table (10) shows that the infill walls in the pinned frame have less strength than infills surrounded by rigid frame with the overall mean PC-to-RC strength ratio of 0.82 with COV of 11.26%. On the other hand, one can suggest that the strength of infill wall in the pinned frame estimated by equivalent strut common model should be multiplied by 0.8. The hypothesis will be evaluated and proved in the following section.

### *4.2. Effect of Number of Bays*

To understand the effect of number of bays on the behavior of infilled steel frame, the main goal is to compare the response of infill wall in the frame with different number of bays. For this purpose, the responses of infill walls in the studied models were determined by calculating the interaction force between infill and frame. Table (11) shows the stiffness and strength of infill contribution of one, two and three-bay infilled frames with rigid and pinned connections. In this table, 2B/1B and 3B/1B indicate the ratios of two-bay to one-bay and

**Table 11.** Effect of number of bays on the stiffness and strength of infill contribution.

| Frame Connection | Bay No. | Stiffness (kN/mm) | Strength (kN) | | | | |
|---|---|---|---|---|---|---|---|
| | | | Drift (%) | | | | |
| | | | 1.35 | 1.67 | 2 | 2.5 | |
| Rigid | 1 | 2.0 | 44.4 | 54.6 | 59.5 | 63.8 | |
| Rigid | 2 | 4.09 | 95.5 | 108.9 | 118.3 | 137.6 | |
| Rigid | 3 | 6.11 | 139.8 | 163.6 | 177.8 | 201.7 | |
| Pinned | 1 | 1.49 | 32.1 | 41.3 | 50.05 | 59.4 | |
| Pinned | 2 | 3.05 | 69.7 | 87.7 | 98.3 | 108.2 | |
| Pinned | 3 | 4.54 | 101.8 | 129 | 148.3 | 168 | |
| | | | | | | | Avg. |
| Rigid | 2B/1B | 2.05 | 2.15 | 1.99 | 1.99 | 2.16 | **2.07** |
| Rigid | 3B/1B | 3.06 | 3.15 | 3.00 | 2.99 | 3.16 | **3.07** |
| Pinned | 2B/1B | 2.05 | 2.17 | 2.12 | 1.96 | 1.82 | **2.02** |
| Pinned | 3B/1B | 3.05 | 3.17 | 3.12 | 2.96 | 2.83 | **3.02** |

three-bay to one-bay specimen characteristics, respectively. It shows that the stiffness and mean capacity of infill wall for three-bay and two-bay models are respectively double and triple those of the single-bay infilled frames. The result is acceptable for both infilled frames with rigid and pinned connections. Therefore, it is concluded that for modeling the infill panel through equivalent strut model in the multi-bay infilled frame, one can apply the same strut as one-bay frame.

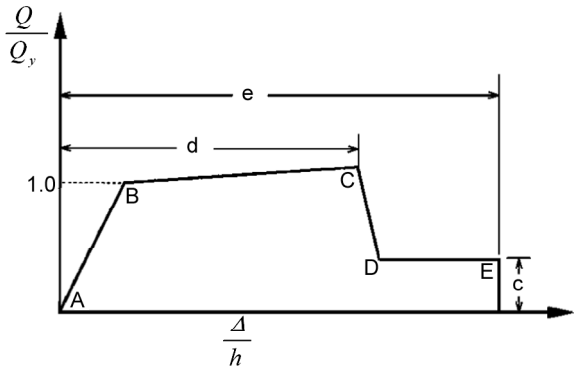


**Figure 8.** Generalized force-deformation relation for infill wall [6].

## 5. Utilizing Equivalent Strut Model

Previous studies [11-12] have shown that the strength and stiffness of multi-bay infilled frame cannot be directly estimated through the behavior of one-bay infilled frame. Kaltakci et al. [23] examined the capability of equivalent strut model to estimate the maximum strength of infilled frames. They concluded that, although the equivalent strut tie method gives rather good results for failure load of one-bay infilled frame, there is 40% difference between the ratio of analytical to experimental failure load, exceeding 40% in two-bay infilled frames. Therefore, in this section, the capability of equivalent strut method in estimation of infill panel behavior in multi-bay infilled frame is examined. For this purpose, the results or abovementioned parametric analysis will be applied to the equivalent compression strut model recommended by Mainstone [4]. Nonlinear pushover analysis is carried out on the infilled frame with diagonal strut using SAP2000 program. In the first step, the characteristics of equivalent strut in a rigid frame are calibrated by the result of FEM accepted in previous section. Then, the verified strut will be evaluated in pinned and multi-bay frames. The Mainstone [4] strut model recommended by FEMA356 [5] and ASCE41-6 [6] is used to evaluate the behavior of the infilled frames. In this model, the infill panel is replaced by a diagonal compression strut in which the strut width is calculated by:

$$w = 0.175(\lambda h)^{-0.4} r_{\inf} \quad (5)$$

where $r_{\inf}$ is diagonal length of infill panel, and $\lambda h$ is relative rigidity of infill to frame defined before. The initial stiffness of infilled frame can be easily determined by performing linear analysis on the frame in which the infill is replaced by the equivalent pinned-joint strut. Figure (8) illustrates the nonlinear behavior of infill wall in which the c, d and e values are recommended by seismic guideline such as ASCE41-06 [6], and $Q_y$ is infill shear strength ($V_{\inf}$), which shall be calculated in accordance with Equation (6):

$$Q_y = V_{\inf} = A_{ni} f_{vie} \quad (6)$$

where $A_{ni}$ is the area of net-mortared section across infill, and $f_{vie}$ is shear strength of masonry infill.

The parameters used to model infill wall via equivalent strut in the rigid connection frame described in previous section are shown in Table (12). It should be noted that $f_{vie}$ was determined based on the experimental shear test of masonry available in [13].

Based on the above-mentioned parameter, the masonry steel frame with rigid connections was modeled with the equivalent strut methodology. The nonlinear static analysis (Pushover) was conducted using commercial program SAP2000. Figure (9) compared the capacity curves of infilled frame obtained by SAP2000 [24] and ABAQUS [14] using equivalent compression strut and finite element methods, respectively. It can be seen that the strut model can appropriately capture the behavior of finite element infilled frame.

**Table 12.** Parameters used for model diagonal struts.

| Elastic Modulus $E_{me}$ (MPa) | Strut Width $w$ (cm) | Strut Thickness $t$ (cm) | $A_{ni}$ (cm$^2$) | $f_{vie}$ (MPa) | $V_{vie}$ (kN) |
|---|---|---|---|---|---|
| 1892 | 30.9 | 9.5 | 1976 | 0.3 | 60 |

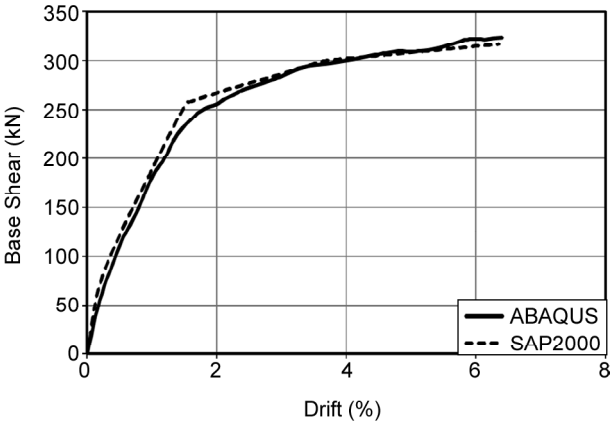


**Figure 9.** Comparison between capacity curves of masonry infilled steel frame with rigid connections using strut and finite element methods

By using the verified strut model in the pinned steel frame, the results obtained by finite element investigation is examined. The pushover curves of infilled steel frame with pinned connection obtained by finite element method and prevalent equivalent strut model are compared in Figure (10a). It shows that the Mainstone model overestimates the stiffness and strength of infilled frame with pinned connections. It was concluded from previous section that the stiffness and strength of infill wall in pinned steel frame are 0.9 and 0.8 times of infill panel in rigid one. Therefore, the strut width and infill shear strength are considered $w = 30.9 \times 0.9 = 27.8$ cm and $V_{vie} = 60 \times 0.8 = 48$ kN, respectively. Figure (10b) illustrates the capacity curve of the infilled pinned frame modeled by modified equivalent strut. It is shown that the proposed diagonal strut model can accurately estimate the stiffness and strength of infilled pinned frame. As a result, to model the infill wall by equivalent diagonal strut in pinned steel frame, Equations (7) and (8) are proposed:

$$w = 0.157(\lambda h)^{-0.4} r_{\text{inf}} \tag{7}$$

$$Q_y = V_{\text{inf}} = 0.8 A_{ni} f_{vie} \tag{8}$$

Multi-bay infilled frames were also modeled through equivalent diagonal strut method and analyzed using SAP2000 [24]. The results are compared with those of finite element analysis in ABAQUS [14] illustrated in Figure (11). It shows that the equivalent strut method can appropriately capture the behavior of multi-bay infilled frame with both rigid and pinned connections.

## 6. Conclusion

Capability of equivalent diagonal strut method for modeling infill wall in pinned connection and multi-bay steel infilled frames is investigated in this paper. For this purpose, the results of finite element analysis were calibrated by experimental test data. A parametric finite element study has been carried out on the influence of connection rigidity and number of bays on the behavior of masonry infilled steel frames using ABAQUS. The results showed that the stiffness and strength of infill panel in pinned frames are 0.9 and 0.8 times of those in rigid frame, respectively. Moreover, the behavior of infill wall in multi-bay frames has a linear relationship with the number of bays. Finally, the results of parametric study showed that the equivalent strut method is capable for modeling infill walls in multi-bay frames; however, it should be improved for pinned connection frames. A new equation was proposed to model the infill panel by equivalent strut in pinned steel frame.

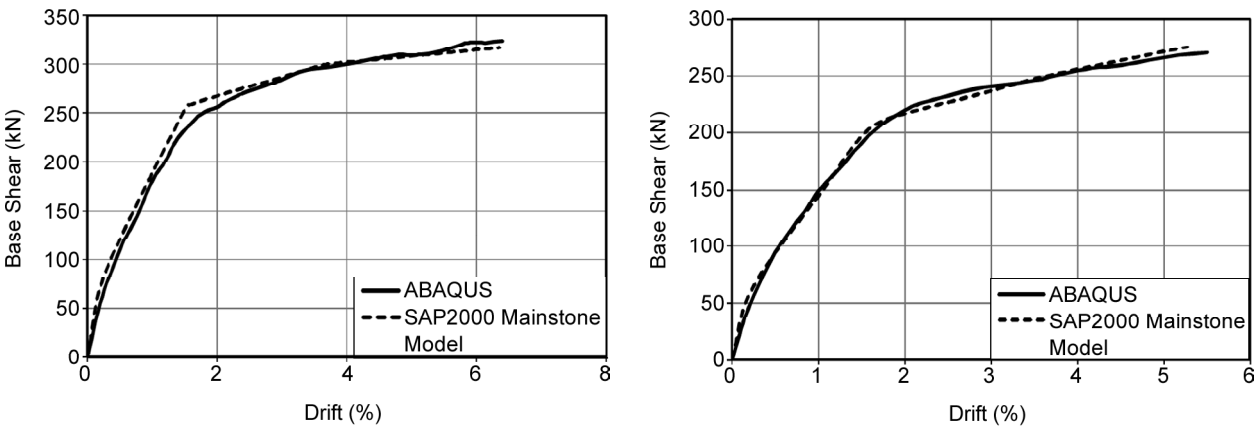


(a) Mainstone and Finite Element Methods

(b) Proposed and Finite Element Methods

**Figure 10.** Comparison between capacity curves of masonry infilled steel frame with pinned connections.

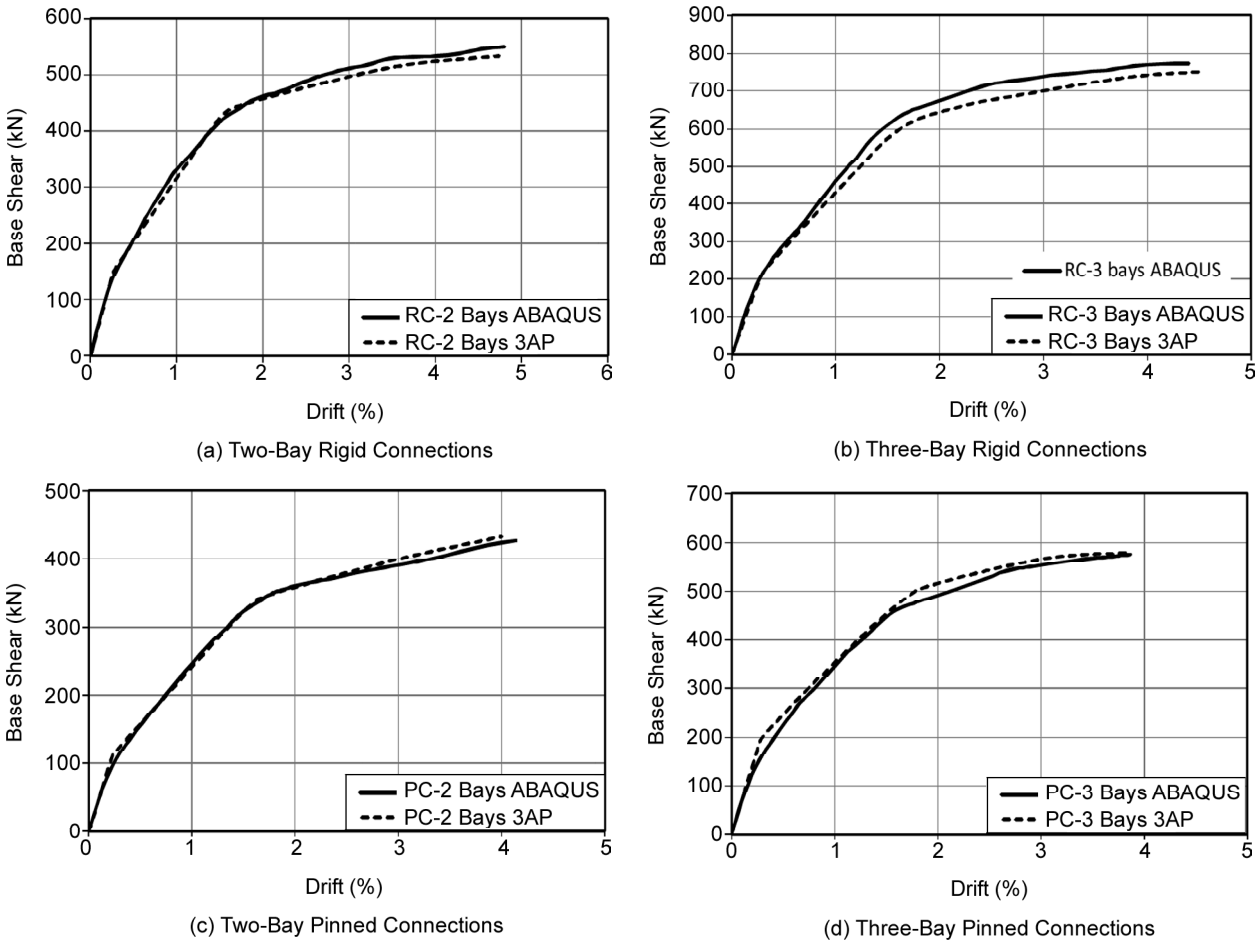


**Figure 11.** Comparison between capacity curves of ABAQUS and SAP.

## Acknowledgments

This study was supported financially by International Institute of Earthquake Engineering and Seismology (IIEES), as well as Organization for Renovating, Developing and Equipping Schools of Iran under grant No. 7386 and 7387.

## References

1. Polyakov, S. (1960) On the interaction between masonry filler walls and enclosing frame when loaded in the plane of the wall. *Translations in Earthquake Engineering*, 36-42.
2. Holmes, M. (1961) Steel frames with brickwork and concrete infilling. *ICE Proceedings*, 473-478.
3. Smith B.S. and Carter, C. (1969) A method of analysis for infilled frames. *ICE Proceedings*, 31-48.
4. Mainstone, R.J. (1971) On the stiffness and strengths of infilled frames. *ICE Proc. Thomas Telford*, **49**(2), 230.
5. Federal Emergency Management Agency (2000) *Prestandard and Commentary for the Seismic Rehabilitation of Buildings*. Report no. FEMA 356, FEMA, Washington, DC.
6. ASCE 41-06 (2006) Seismic rehabilitation of existing buildings. *American Society of Civil Engineers*, Virginia: Reston.
7. Dawe J. and Seah, C. (1989) Behaviour of masonry infilled steel frames. *Canadian Journal of Civil Engineering*, **16**, 865-876.
8. Flanagan R.D. and Bennett R.M. (1999) In-plane behavior of structural clay tile infilled frames. *Journal of Structural Engineering*, **125**, 590-599.
9. Motovali Emami, S.M. and Mohammadi, M. (2017) Effect of frame connection rigidity on the behaviour of infilled steel frames. *Journal of Constructional Steel Research* (under review).
10. Murthy, C. and Hendry, A. (1996) Model

experiments in load bearing brickwork. *Building Science*, **1**, 289-298.

11. Mosalam, K.M., White, R.N., and Gergely, P. (1997) Static response of infilled frames using quasi-static experimentation. *Journal of Structural Engineering*, **123**, 1462-4169.

12. Al-Chaar, G., Issa, M., and Sweeney, S. (2002) Behavior of masonry-infilled non-ductile re-inforced concrete frames. *Journal of Structural Engineering*, **128**, 1055-1063.

13. Motovali Emami, S.M. (2017) *Effect of Vertical Load, Number of Bays and Connection Ri-gidity of the Frame on the Seismic Behavior of Infilled Steel Frames*. Ph.D. Thesis, International Institute of Earthquake Engineering and Seismology (in Persian).

14. Habbit Karlsson & Sorensen Inc. (2014) *ABAQUS Theory Manual Version 6.14.*

15. Motovali Emami, S.M. and Mohammadi, M. (2016) Influence of vertical load on in-plane behavior of masonry infilled steel frames. *Earthquakes and Structures*, **11**, 609-627.

16. Lubliner, J., Oliver, J., Oiler, S., and Onate, E. (1989) A plastic-damage model for concrete. *International Journal of Solids and Structures*, **25**, 299-329.

17. Lee, J. and Fenves, G.L. (1998) Plastic-damage model for cyclic loading of concrete struc-tures. *ASCE Journal of Engineering Mechanics*, **124**, 892-900.

18. Dugdale, D.S. (1960) Yielding of steel sheets containing slits. *Journal of the Mechanics and Physics of Solids*, **8**, 100-104.

19. Needleman, A. (1987) A continuum model for void nucleation by inclusion debonding. *Journal of Applied Mechanics*, **54**, 525-531.

20. Bolhassani, M., Hamid, A.A., Lau, A.C., and Moon, F. (2015) Simplified micro modeling of partially grouted masonry assemblages. *Construction and Building Materials*, **83**, 159-173.

21. Standard No. 2800 (2005) *Iranian Code of Practice for Seismic Resistant Design of Buildings*. Third Revision, Building and Housing Research Center, Iran (in Persian).

22. ASCE 41-13 (2012) *Seismic Rehabilitation of Existing Buildings*. American Society of Civil Engineers; Virginia: Reston.

23. Kaltakci, M., Koken, A., and Korkmaz, H. (2006) Analytical solutions using the equivalent strut tie method of infilled steel frames and experimental verification. *Canadian Journal of Civil Engineering*, **33**, 632-638.

24. CSI, SAP2000 V. 14.1 (2010) *Integrated Finite Element Analysis and Design of Structures Basic Analysis Reference Manual*. Computers and Structures, Inc., Berkeley, California, USA.